공학석사 학위논문

Molecular simulation informed viscoelastic constitutive model for amorphous polymer and its incremental formulation

비정질 고분자의 분자 시뮬레이션 기반 점탄성 구성방정식과 증분 정식화 유도

2021 년 2 월

서울대학교 대학원

항공우주공학과

정 지 원

Molecular simulation informed viscoelastic constitutive model for amorphous polymer and its incremental formulation

비정질 고분자의 분자 시뮬레이션 기반 점탄성 구성방정식과 증분 정식화 유도

지도 교수 윤 군 진

이 논문을 공학석사 학위논문으로 제출함
2020 년 12 월

서울대학교 대학원
항공우주공학과
정 지 원

정지원의 공학석사 학위논문을 인준함
2020 년 12 월

위 원 장 김 도 년 (인)

부위원장 윤 군 진 (인)

위 원 이 복 직 (인)

Abstract

Molecular simulation informed viscoelastic constitutive model for amorphous polymer and its incremental formulation

Jiwon Jung
Department of Aerospace Engineering
The Graduate School
Seoul National University

This thesis aims to develop a viscoelastic constitutive equation of elastomers that reflects the molecular characteristics. In the viscoelastic constitutive equation, each polymer characteristic variable is obtained from the primitive path analysis, the molecular model's initial condition, and the coarse-grained molecular dynamics (MD). To compose a coarse-grained model of the elastomer, the energy renormalization method was employed. The molecular simulation is accelerated through the energy renormalization method,

and the same level of precision as the conventional all-atom MD is conserved by controlling the interaction parameters between molecules according to temperature. However, since the existing method did not consider the correlation between the two parameters included in the potential, the multi objective optimization algorithm was adopted and verified. Furthermore, the viscoelastic properties of the elastomer were obtained from the viscoelastic constitutive equation. Since the previous literature did not report the incremental formulation for the implicit finite element analysis, the incremental formulation of the viscoelastic constitutive equation and the tangent stiffness matrix's derivation was suggested. Moreover, the study on crosslink effect and a parametric study were conducted by investigating the effect of the variables included in the viscoelastic constitutive equation on the dynamic properties.

Keywords: Multiscale simulation, molecular dynamics, viscoelastic polymer, elastomer, finite element analysis

Student Number: 2019-20587

Table of contents

List of figures

List of tables

1. Introduction

1.1. Background and motivation

In contemporary cutting-edge industries, composites are a widely studied field of research for enhancing performance efficiencies. The most commonly used composites for structure consist of the reinforcement with high stiffness and the matrix with high toughness that holds reinforcements. Due to their high strength with light weights, they are utilized in various fields, including aerospace, marine, fuel tanks, etc. However, since they show anisotropic thermo-mechanical characteristics and unique failure modes such as delamination, it makes the analysis of composites more difficult. For composites, the simple rule of mixture, failure criteria like Tsai-Wu, Tsai-Hill [1], and Mori-Tanaka [2] homogenization methods were developed as pioneering researches for composites.

Furthermore, with the discovery of nanoscale reinforcements including carbon nano tubes (CNT) and graphenes, more variables were considered. Therefore, the importance of the computer simulations describing physical phenomena without experiments has

been elucidated to reduce economic and temporal resources consumed during the classical trial-and-errors.

Structural analysis with computer simulations has been mainly conducted with macroscale continuum finite element analysis (FEA). Expanded from elastic material analysis, several material models to depict nonlinearities generated from viscoelasticity and hyperelasticity in FEA have been suggested. As the simplest model, the Generalized Maxwell Model and the Neo-Hookean model are commonly used to analyze viscoelasticity and hyperelasticity, respectively. However, the aforementioned models were empirically developed, and they contain mathematical parameters that do not have any physical meanings. Therefore, to apply such models to FEA, experiments should be executed to fit mathematical parameters and cannot reflect the effects of the matrix's molecular structures. Thus, to study polymer nano-composites with diverse molecular srtuctures, the molecular dynamics (MD) simulations were developed.

From MD simulations, material properties are calculated through the Newton equation of force fields defined by the interaction

between atoms. Force field terms in all-atom scale MD can be classified into two categories: (1) non-bond terms, including Van der Waals interactions and coulomb forces, (2) and bond terms including bond, angle, dihedral, improper, etc., which acts between chemically bonded atoms. Since MD simulations predict physical behavior at the molecular scale, researches for several phenomena such as phase change and interphase properties that were difficult to study in experimental scale have been attempted in the MD simulation. However, in MD simulation, it has limitations that they are conducted at the nano length and time scale, and they have substantial discrepancy from macroscales. Therefore, to compensate for limitations with nanoscale MD and macroscale FE simulations, several researches to bridge between nano and macroscales were conducted.

To study the viscoelasticity of elastomer in MD scale, the extensive time to observe time-dependent properties of the polymer is consumed. Thus, to reduce computational resources during MD simulations, the coarse-grained MD was developed. In coarse-grained MD, several adjacent atoms were combined into a single bead,

and the overall degree of freedom in the molecular system is reduced. However, since the computation accuracy is sacrificed, several methodologies to find proper coarse-grained MD potential matching with all-atom simulations were developed [3-6]. The coarse-grained MD can be classified into the degree of coarse-graining. At the finest level, TraPPE(UA) potential [3] combines a carbon atom and adjacent chemically bonded hydrogen atoms, and they were called united-atom force fields. In a molecular level of coarse-graining, the Iterative Boltzmann Inversion (IBI) method [4] is commonly adopted, and even several molecules were combined in elastomer studies with MD [6]. Even though IBI had the strength to describe the structural properties, some results from non-equilibrium MD simulations such as mechanical moduli and thermomechanical properties were not matched since frictions between polymer chains were diminished. Therefore, to compensate for such effects, the dissipative particle dynamics method (DPD) [7, 8] was adopted by adding non-conservative forces between beads. The temperature-transferable energy renormalization method was developed to develop force fields for thermodynamic studies [9, 10].

Even by such efforts to expand MD into the mesoscale, they are conducted at the microscales and have a huge discrepancy with experimental scale.

Several constitutive equations were developed in the analysis of viscoelasticity and hyperelasticity of elastomers with FEA that can directly reflect the molecular structure difference and include physical parameters rather than empirically developed mathematical parameters. As pioneering research for the elastomer hyperelastic model, Arruda-Boyce developed an 8-chain network model for crosslinked elastomers [11]. For the viscoelastic constitutive equation, the Bergström-Boyce model [12] and microsphere model [13] were proposed. Moreover, the expansion of classical FEA into multi-scale micro-morphic analysis was also tried to bridge between nano and macroscale. Park et al. [14, 15] studied the polymer's inhomogeneous deformation by applying SS curves from MD at the microscale and experimental results at the macroscale. They showed that the size of microscale affects the strain rate at the microscale and fast strain rate over $10^8 \sim 10^{10}/s$ in MD has been accomplished. Tang et al. [16] developed 2D model of elastomer

where Arruda–Boyce [11] hyperelasticity for crosslinked network in macroscale and viscoelasticity for free chain network in microscale were adopted. In 2012, Li et al. [17] developed a molecular simulation simulation–informed viscoelastic constitutive equation with Doi–Edward's model developed based on the tube theory [18, 19] and where all the parameters have exact physical meanings. In the tube theory, motions of each polymer chain in the free chain network is assumed to move as moving in the virtual tube by constraints from neighborhood chains.

The viscoelastic model established from the tube theory contains parameters oriented from polymer dynamics, polymer physics, and polymer chemistry. Parameter from polymer dynamics is determined from coarse–grained MD simulation, and parameters from polymer chemistry are determined from polymerization condition when manufactured. Polymer physics parameters are based on tube theory, and it can be obtained from primitive path analysis code (Z1 code) developed by M. Kröger [20]. In this paper, we performed coarse–grained MD and primitive path analysis with Z1 code. During the coarse–grained MD, the energy renormalization

method was adopted modified with the multi-objective optimization algorithm [21]. Then, by plugging parameters from the molecular simulations into the viscoelastic constitutive equation, the viscoelastic properties of polymer, i.e., dynamic modulus and $\tan\delta$ were obtained, and the effects of molecular parameters on them were investigated. Moreover, the crosslink effect on the polymer viscoelasticity, incremental formulation, and the derivation of tangent stiffness to apply the 1D Doi-Edward viscoelastic model on ABAQUS user subroutine UMAT was studied in this thesis. Through expansion of the formulation to 3D viscoelastic constitutive equation with arbitrary deformation gradients, application to general implicit FEA is expected.

1.2. Organization of the thesis

This thesis is organized as follows. In the next section, the molecular modeling of the polyisoprene model is described (section 2.1). A review of the coarse-grained potential with the energy renormalization method and an investigation of the correlation effect between two renormalization parameters is discussed (section 2.2).

In Section 2.3, considering the correlation effect, the multi-objective optimized coarse-grained potential is suggested and verified. Then, the primitive path analysis is conducted, and the characteristic molecular parameters are proposed in Section 2.4. Section 3 explains the application of the viscoelastic constitutive equation to FEA. The incremental formulation of the viscoelastic Cauchy stress and material tangent stiffness is derived in Section 3.1. The verification of the formulation by comparison with direct calculation of Cauchy stress is discussed in Section 3.2. Then, the parametric study on the viscoelastic constitutive equation was conducted and described in section 3.3. The conclusions of this thesis and plans for future works are suggested in Section 4.

2. Molecular simulation methods and analysis based on the tube theory

To compose tube theory-based viscoelastic constitutive equations, polymer parameters from molecular simulations with coarse-grained MD and PPA should be conducted. From the coarse-grained MD, the self-diffusivity (D_c) is calculated as the polymer dynamics oriented parameter. The molecular model for the calculation of coarse-grained potential of the polyisoprene (PI) was generated through the anionic polymerization algorithm which was modified from the previous work of the free radical polymerization algorithm [22]. Through the PPA, molecular characteristic parameters such as tube diameter (a), tube length (L), Kuhn length, are obtained. The parameters from polymer chemistry, the average number of monomers in chains (N) and the number of chains in a unit volume were determined from the initial condition of the molecular models. For the analysis of viscoelastic properties, six molecular models were built. Two kinds of molecular models include (1) 20 chains with 2000 monomers in each chain, and (2) 10 chains with 4000 monomers in each chain to have an equal number of total monomer beads, Each kind of models contain disulfide crosslinkers

with a weight percentage of 0%, 1%, 2%. The center of the mass of each isoprene molecule was mapped into a single bead coordinate in the simulations depicted in Figure 1 while sulfur atoms were calculated in all-atom scale.

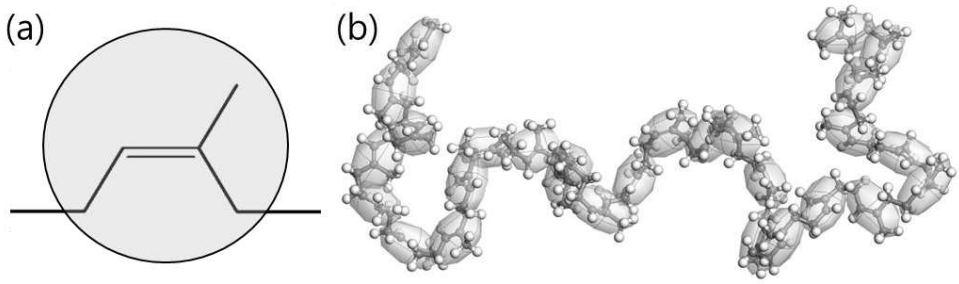

Figure 1 (a) Description of the isoprene molecule combined into a single bead in the coarse-grained model and (b) an illustration of the single PI chain.

2.1. Molecular modeling of the polyisoprene model for coarse-grain MD force field.

To build a molecular model of PI, the anionic polymerization algorithm was adopted. Modified from the free radical polymerization algorithm [22], the anionic polymerization algorithm was accomplished by removing the termination reaction when two other reactive atoms met. Before the polymerization, the initial model had 2000 isoprene molecules, and ten initiators were included, randomly

dispersed. In this thesis, the anionic polymerization algorithm was conducted as follows: (1) the initiation step in which initial reactive atoms were activated in the initiator, (2) and the propagation step in which the chains grew, new monomers were reacted with the chain ends. In this algorithm, the propagation step was assumed to progress in a head–to–tail direction. The polymerization algorithm was conducted with the commercial molecular dynamics software, Materials Studio 2017 R2 [23]. The initiation step was represented in the simulation by randomly dispersing the initiator with reactive atoms within the monomers using the amorphous cell module included in the software. Two types of reactive atoms and potential reactive atoms were assigned in each molecule to describe the propagation steps of the anionic polymerization. The reactive type 1 atoms were reactive chain ends, and the reactive type 2 atoms were head atoms in each molecule. When two different types of reactive atoms were within a certain cutoff distance, they were reacted and form new chain ends. Then, the potential reactive atom site located at the tail of the molecule was changed into reactive site 1. As the propagation step was operated iteratively, the free chain network of the polymer

was formed. To compensate the artificial bond formation from the propagation step, 2000 steps of the geometry optimization with the conjugate gradient method were performed for every ten steps. The propagation steps were iteratively done until 95% of the monomers were reacted. If any set of different atom types were not found, the cutoff distance was increased by 0.5Å from 7Å to 11Å. Then, 2ps of NPT ensemble under 1atm, 300K was applied. After the polymerization, the PI model of $0.859 g/cm^3$ with 95% of total monomers were reacted, was generated. The polymerization procedures were operated with COMPASS II force field [24, 25], and the overall scheme and the flow chart is shown in Figure 2 and Figure 3, respectively.

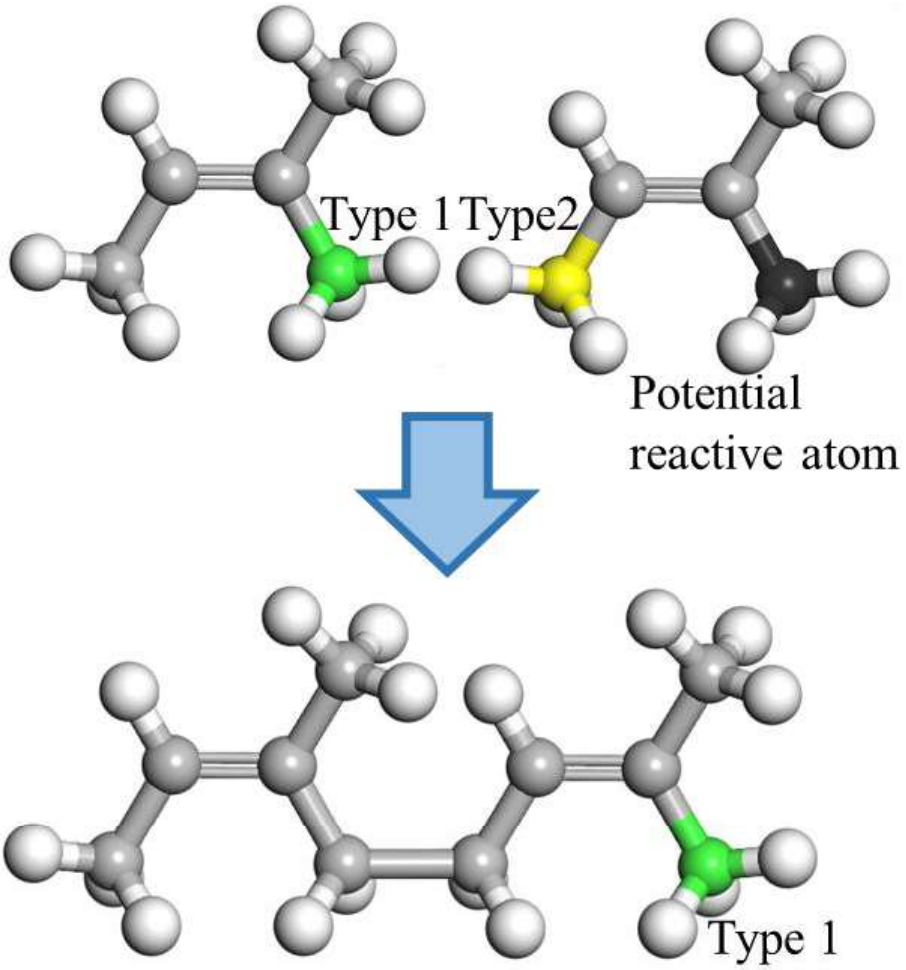

Figure 2 Illustration for the propagation step in the anionic polymerization algorithm.

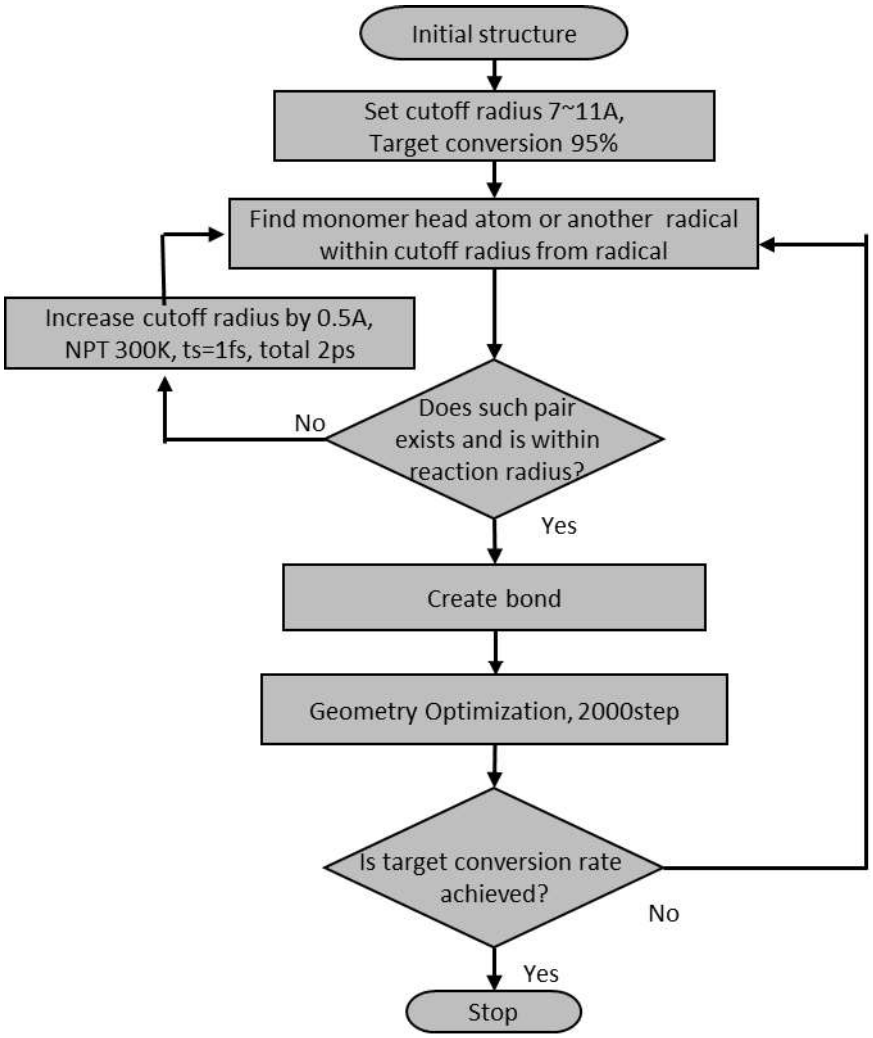

Figure 3 Flow chart for the anionic polymerization algorithm.

2.2. Investigation on the energy renormalization method

2.2.1. Literature review of the energy renormalization method

The coarse-grained MD method with the energy renormalization method for glass-forming liquids was first proposed in 2017 by Xia et al. [9]. Based on the Adam-Gibbs theory, coarse-grained force field parameters were controlled as functions of the temperature. In the energy renormalization method, nonbonded interactions between beads were expressed as following Eq. (1).

$$V(r) = \varepsilon\left[2\left(\frac{\sigma}{r}\right)^9 - 3\left(\frac{\sigma}{r}\right)^6\right], \qquad r < r_c \tag{1}$$

where ε_0 and σ_0 determine the energy well depth and equilibrium distance. r_c is the cutoff distance where non-bond potentials were only calculated for pair of beads within r_c, and it was set as 15Å. In this thesis, 9-6 Lennard Jones form was adopted while 12-6 Lennard Jones form of the potential was adopted in the literature [9]. To control ε and σ, the renormalization parameters α and β was multiplied on the initial Lennard Jones parameter ε_0 and σ_0 which were obtained from the Inverse Boltzmann method. The renormalization parameters were expressed as functions of the

temperature. To obtain α, it was found by matching properties from coarse-grained properties with all-atom properties in three different temperature regimes. In the Arrhenius regime ($T > T_a$) where molecular properties follow the Arrhenius equation, α was found by matching the self-diffusivity of the molecular system, which was calculated from the mean square displacement (MSD) as shown in Eq. (2).

$$D_c = \lim_{t\to\infty} \frac{1}{6t} \langle r_{CM}(t) - r_{CM}(0) \rangle^2 = \lim_{t\to\infty} \frac{1}{6t} MSD \qquad (2)$$

where $r_{CM}(t)$ is the coordinate of beads at time t and $r_{CM}(0)$ is the initial coordinate of beads. The Arrhenius temperature T_a was determined as the point where the D_c was escaped from the linear relationship in the Arrhenius plot. In the rubbery regime ($T_a > T > T_g$) where the polymer system shows rubbery characteristics, α was determined by matching the segmental relaxation time τ_d with all-atom models. The glass transition temperature T_g was determined as 201.1K where the thermal expansion coefficient changes during the cooling down simulation [26]. In the glassy regime ($T_g > T$) where the polymer system shows glassy characteristics, α was determined by matching the shear stress curve, since the mobility of the polymer

system is restricted. After fitting α with the above procedures, β was then found by matching density with the all-atom model. As a result, the renormalization parameters were reported as Eq. (3) and Eq. (4) in the literature [9].

$$\alpha(T) = \frac{\alpha_a - \alpha_g}{1 + exp[-k(T - T_T)]} + \alpha_g \quad (3)$$

$$\beta(T) = aT + b \quad (4)$$

where α_a, α_g are α values at the Arrhenius regime and the glassy regimes, and k, T_t, a, b are constants. However, there were no considerations about correlation effects of α and β even though the density of the system can strongly affect MSD and shear stress in the literature [9]. Therefore, the multi-objective optimized coarse-grained potential in the Arrhenius regime is proposed in this thesis. Through the multi-objective optimization algorithm, MSD and density can be matched simultaneously, considering the correlation effect.

2.2.2. Correlation effects between renormalization parameters

In this section, the correlation effect between the renormalization parameters was investigated in the Arrhenius regime and the glassy regime. Before studying the correlation effect, the initial potential values ε_0, σ_0 were obtained, and T_a, T_g were determined to establish each temperature regime.

To obtain ε_0 and σ_0, the Inverse Boltzmann Method (IBM) [4, 9] was conducted in 300K. In the IBM, the non-bond potential is obtained from the inverse Boltzmann of the radial distribution function g(r), and the bond length distribution between beads d(r) as Eq. (5).

$$V(r) = -k_B T \ln g(r) \tag{5}$$

where k_B is the Boltzmann constant, and T is the temperature. Similarly, the bond potential is obtained from the inverse Boltzmann of the bond length distribution between beads. As the bond distribution is fitted as the Gaussian distribution, the harmonic function form of the bond potential is obtained as Eq. (6) and Eq. (7).

$$d(r) = \exp\left(-\frac{K(r - r_0)^2}{k_B T}\right) \tag{6}$$

$$V'(r) = -k_B T \ln d(r) = K(r - r_0)^2 \tag{7}$$

where K is the constant for the strength of the bond and r_0 is the equilibrium bond distance. The model with 1000 isoprene monomers was generated for the calculation of g(r) to remove bond length effects. To calculate bond length distribution d(r), the model with 10 chains which has 100 monomer were polymerized each, was generated, The g(r) and d(r) were calculated by averaging 100 trajectories obtained from 1ns NVT ensemble after 100ps of NPT ensemble under 1atm, 300K condition to converge the density. The simulations to get trajectories were conducted with the materials studio and COMPASS II force field. The Andersen thermostat [27] and the Berendsen barostat [28] were applied to control the pressure and the temperature. For calculating the bond length, the distance between the adjacent centers of carbon-carbon bonds connecting between isoprene molecules, and the distribution functions and initial potentials from IBM are shown in Figure 4. The initial potential parameter ε_0 and σ_0 were determined as the value at the minimum point of the inverse Boltzmann of g(r).

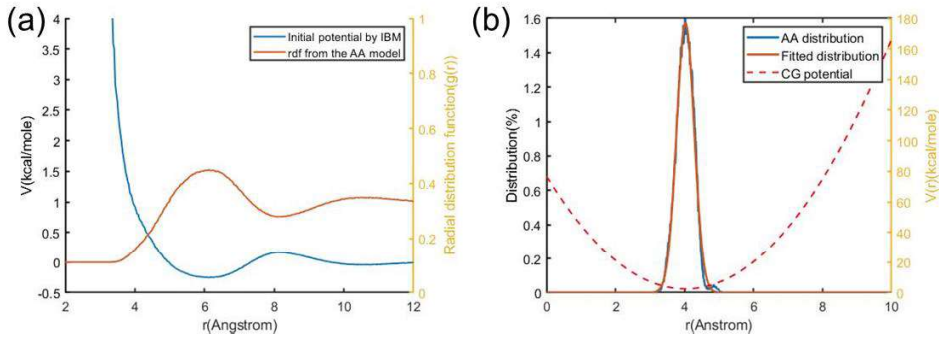

Figure 4 (a) The radial distribution function g(r) and initial non-bond potential obtained from the Inverse Boltzmann of g(r). (b) The bond length distribution fitted with the Gaussian distribution and the harmonic form of the bond potential.

To determine T_a, D_c was calculated for 450K~1000K condition, and the Arrhenius plot was drawn. As expressed in Figure 5(a), 750K was determined as T_a where the linear relationship between the logarithm of D_c and reciprocal of the temperature was escaped. The MSD in each temperature condition was calculated from the 1ns simulation after the 800,000 steps of NPT and 500,000 steps of NVT ensemble to converge density and relax the system. Moreover, to obtain T_g, the cooling down simulation with $1.0 \times 10^{11} K/s$ was conducted and the relationship between the density and the temperature was plotted. As shown in Figure 5(b), 201.1K was determined as T_g where the gradients in the figure changed. Molecular simulations under this part including the calculation of T_a, T_g was conducted with the molecular dynamics software,

LAMMPS [29], and Nose–Hoover thermostat and barostat [30] were employed.

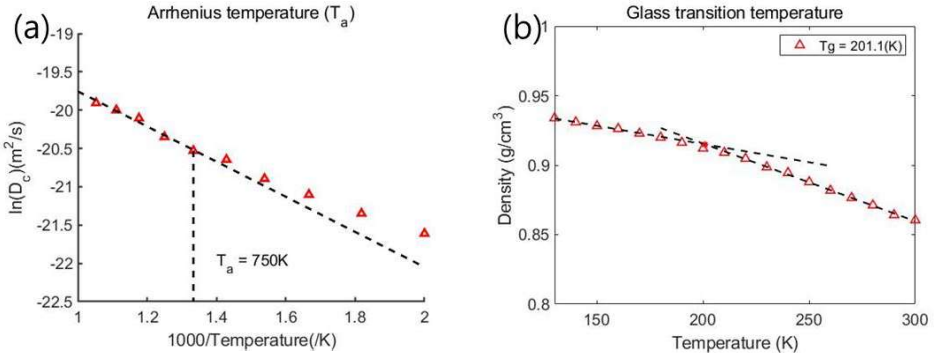

Figure 5 (a) The Arrhenius temperature ($\mathbf{T_a}$) determined as a point where the linear relationship escaped in the Arrhenius plot of $\mathbf{D_c}$, (b) and the glass transition temperature ($\mathbf{T_g}$) determined as a point where the thermal expansion coefficient changes.

To investigate the correlation effect between two renormalization parameters, the effect of the renormalization parameters on each other's fitting variables was investigated in the Arrhenius regime and the glassy regime. In the Arrhenius regime (850K), the specific volume of the molecular system was calculated for varying $\alpha = 2{\sim}4$ under constant $\beta = 1.3$, and conversely, the MSD was calculated for varying $\beta = 1.1{\sim}1.4$ under constant $\alpha = 2$. As shown in Figure 6, the increase of MSD for increasing β and decrease of the specific volume for increasing α was observed.

Since the mobility calculates MSD, MSD was increased in extensive volume conditions led by larger β values. Moreover, when α and the energy well depth were increased, it strengthened the interaction forces between molecules, and therefore, the specific volume of the molecular system had decreased.

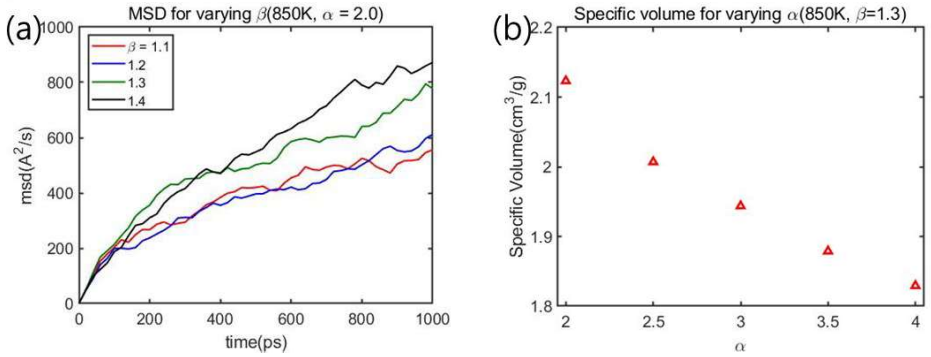

Figure 6 (a) MSD calculated for varying **α** under constant **β** condition, (b) and the specific volume calculated for varying **β** under constant **α** condition at 850K

Furthermore, in the glassy regime (160K), the shear stress was calculated for varying $\beta = 1.0 \sim 1.6$ under constant $\alpha = 3.5$. Conversely, the specific volume was calculated for varying $\alpha = 3.0 \sim 5.0$ under constant $\beta = 1.6$ condition. The pure shear deformation with $1.0 \times 10^8/s$ of strain rate was applied to obtain shear stress of the system. As shown in Figure 7, higher shear stress was observed in low β conditions since molecules are more densely packed in low specific volumes, and therefore, frictions between

polymer chains increase. The calculation of the specific volume showed a similar trend with the results in the Arrhenius regime. However, the dependency of the specific volume on α was smaller than the dependency in the high-temperature condition since the molecules are sufficiently condensed each other.

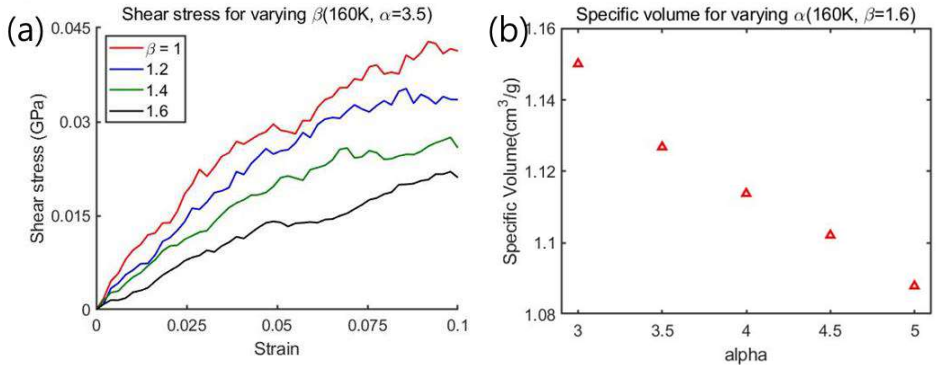

Figure 7 (a) The shear stress curves calculated for varying **α** under constant **β** condition, (b) and the specific volume calculated for varying **β** under constant **α** condition at 160K

As discussed above, it was found that two renormalization parameters were correlated, and they affect each other's fitting parameters. Therefore, unlike previous literature [9], α and β should not be found independently but matched simultaneously. To match MSD and the density simultaneously in the Arrhenius regime, the multi-objective optimization algorithm was adopted. Since the

correlation effect was smaller in the glassy regime, α was found by matching the shear stress curves, and then β was obtained.

2.3. Multi-objective optimized coarse-grained MD potential

2.3.1. Optimization results and parameter function

To obtain a suitable solution for α and β in the Arrhenius regime, a multi-objective optimization algorithm was applied to find the set of parameters that match the MSD and density simultaneously as the results from all-atom simulations. The reference all-atom data was calculated from the identical procedure conducted for the investigation of the correlation effect. To make reference all-atom data more precise, the all-atom simulations were conducted five times and three times then, averaged for calculating MSD and shear stress, respectively. The non-dominant sort genetic algorithm (NSGA-II) [23] was applied for the algorithm that uses two coefficients of decision variables (α, β) and two objective functions (root-mean-square error and density error between MSD curves. The optimization algorithm was operated for 50 generations and 20

populations. The mutation parameter was set as 50 to prevent solutions from converging into local minima. The boundaries for the optimized decision variables were set as $\alpha \in [2.0,4.0]$ and $\beta \in [0.8,2.5]$ where the simulations were stable. In the Arrhenius regimes, the optimization algorithm was operated four times at each temperature condition, 750K to 950K with 50K intervals. After the optimization, some solutions with large error, 0.03g/cm^3 for density and 100$Å^2/ps$ for root mean square error for MSD curves were excluded. The optimized solutions of α and β are plotted in Figure 8.

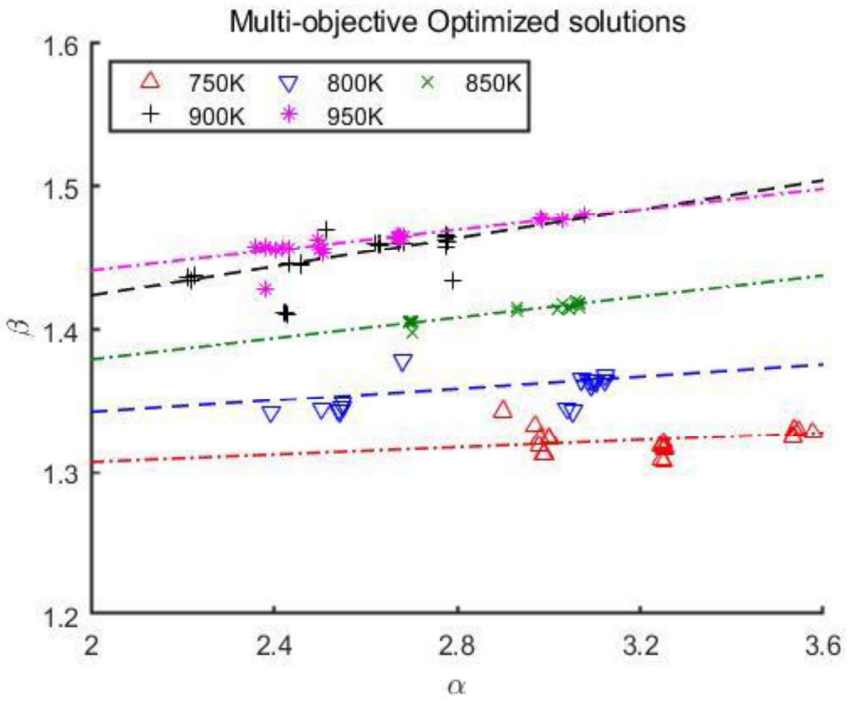

Figure 8 Multi-objective optimized solutions of **α** and **β** in the Arrhenius regime found by matching MSD and density with the all-atom results.

As shown in the graph, the optimized solutions in each temperature were expressed as linear sets. Such solutions are compatible with the correlation effect that higher β is necessary for higher α conditions to compensate for increased MSD and density. In the constant α condition, higher β values were needed in the higher temperature condition since the molecular model has a higher specific volume. Therefore, more considerable equilibrium distances between beads should be accomplished to match the specific volume. To find

α and β as functions of the temperature, a specific point over linear sets of solutions should be selected. Since arbitrary points over the lines can be solutions, the constant $\alpha = 3.0$ where the most solutions are concentrated was selected in this thesis to compose α(T) as a function of the temperature in the form of Eq. (3). In the glassy regime, α was found by matching the shear stress. As expressed in Figure 9, a constant value of $\alpha = 4.5$ found for the glassy regime.

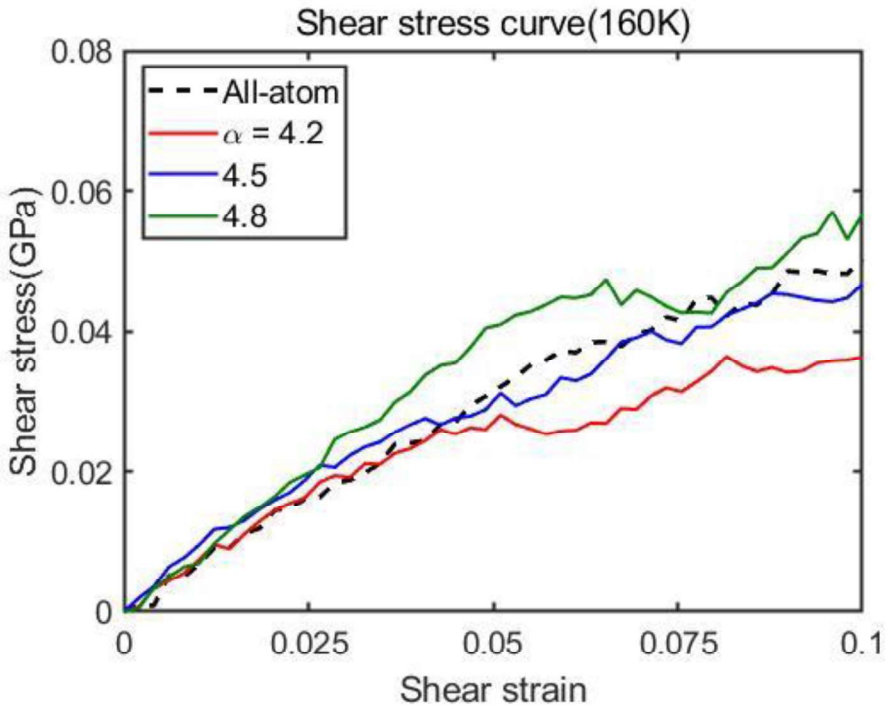

Figure 9 $\alpha = 4.5$ by matching shear stress curves with the all-atom model results in the glassy regime.

To determine α values in the rubbery regimes, α was fitted as a function of the temperature by substituting $\alpha_a = 3.0$ and $\alpha_g = 4.5$ into Eq. (3). Therefore, α(T) was obtained as a sigmoidal function as shown in Figure 10(a). Then, under the condition of α obtained, β was found by matching the density with the all-atom model. As a result, β was found as the form of Eq. (8). The detailed parameter values of α(T) and β(T) are listed in Table 1.

$$\beta(T) = \frac{\beta_a - \beta_g}{1 + \exp[-k(T - T_T)]} + \beta_g \qquad (8)$$

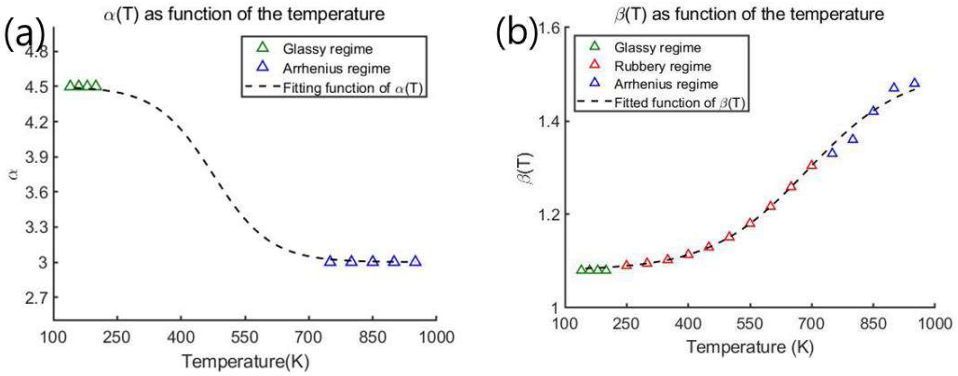

Figure 10 (a) α(T) fitted with the sigmoidal function as Eq. (3), (b) β(T) found by matching the density with all-atom results under $\alpha(T)$ condition obtained from (a).

Table 1 Constant value of the renormalization parameters $\boldsymbol{\alpha(T)}$, $\boldsymbol{\beta(T)}$. Their functional forms are shown in Eq. (3) and Eq. (8), respectively.

Parameter	Value at the glassy regime (α_g, β_g)	Value at the Arrhenius regime (α_a, β_a)	k(/K)	Transition temperature ($\mathbf{T_T}$, K)
α(T)	4.5	3.0	0.015	475
β(T)	1.08	1.51	0.0085	690

2.3.2. Verification of the potential

In section 2.3.1, α(T) in the rubbery regime was fitted with the mathematical function, Eq. (3), and should be verified. Therefore, in the rubbery regime (250K~700K), MSD was calculated and compared with those from all-atom simulations. As expressed in Figure 11, the self-diffusivity coefficient D_c was matched between the coarse-grained model and the all-atom model. It implies that the coarse-grained potential composed by the procedures in the above sections was successfully built to mimic the all-atom simulations.

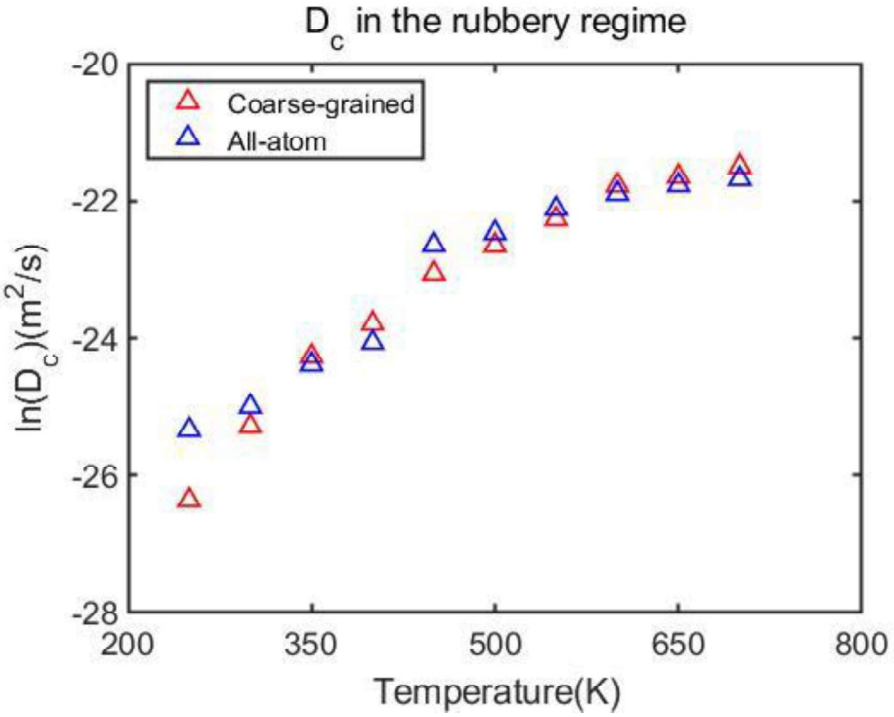

Figure 11 Self-diffusivity coefficient $\mathbf{D_c}$ calculated from MSD compared between the coarse-grained model and the all-atom model to verify the coarse-grained potential.

2.3.3. Coarse-grained potential of the crosslinked elastomer

For the study of the crosslinked elastomer, the coarse-grained potential parameters of the sulfur are necessary. Non-bond potentials and the bond potentials of the sulfur-sulfur interactions and the isoprene-sulfur interactions were obtained. Since sulfur atoms were calculated for each atom in this study, parameters

associated with sulfur–sulfur interactions were obtained from the all–atom parameters in the polymer consistent force field (PCFF) [31]. The bond potential's quartic form was adjusted into harmonic form to match isoprene molecules' interactions. To obtain interactions between sulfur atoms and isoprene molecules, a combination rule for different atoms from the PCFF was applied.

To build the crosslinked model of the polyisoprene, the models with 1%, 2% weight percentage of disulfide crosslinkers randomly dispersed, was generated. From the initial model, disulfide and adjacent isoprene molecules were bonded by a crosslink algorithm with iterations [32]. In the crosslink algorithm, the pair of isoprene molecule and sulfur atom was found within a certain value of cutoff radius (7Å), then bonded. The bond trial was tried iteratively until 100% of the sulfur atoms were bonded. The figure of the coarse–grained model of the crosslinked polyisoprene is shown in Figure 12.

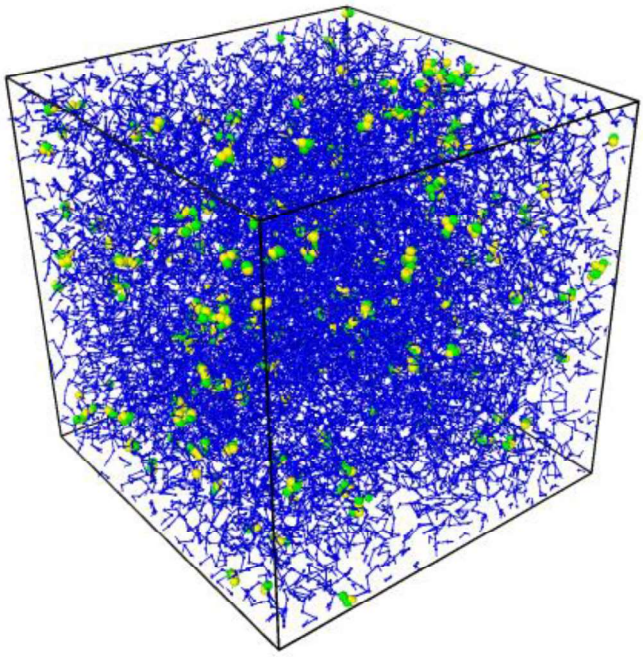

Figure 12 Illustration of the coarse-grained model of the 100% crosslinked model, where blue particles are isoprene molecule, yellow particles are isoprene molecules bonded to disulfide crosslinkers, and green particles are sulfur atoms.

2.4. Primitive path analysis

The polymer physics-oriented parameters included in the Doi-Edward's viscoelastic constitutive equation were obtained from the primitive path analysis (PPA). Through PPA, the free chain network of the polymer is analyzed based on the tube theory. In the tube theory, the movement of the polymer chains are described as in

the virtual tube, since the entanglements with adjacent polymer chains restrict the movement. The viscoelasticity of the polymer system is characterized by properties of the tube such as the tube diameter(a), the tube length(L, i.e., the primitive path length), and the Kuhn length (b), which are the outputs of the PPA. In this thesis, PPA was executed through Z1 code [20, 33], and it was operated as following steps: (1) The ends of the polymer chains were fixed, and each backbone bond in polymer chains were replaced by infinitesimally thin and unable to be crossed lines. (2) Then, their paths were iteratively reduced and converged into the final state. Finally, the shortest path connecting chain ends restricted by the entanglements with adjacent chains, is determined as a primitive path. After the PPA is operated on the polymer system's free chain network, it was simplified, as illustrated in Figure 13. For the crosslinked model, the same PPA parameters as the free chain model were used. The difference of the D_c was considered for the analysis of the polymer viscoelasticity. The polymer characteristic parameters obtained from the PPA and the coarse-grained MD are listed in

Table 2.

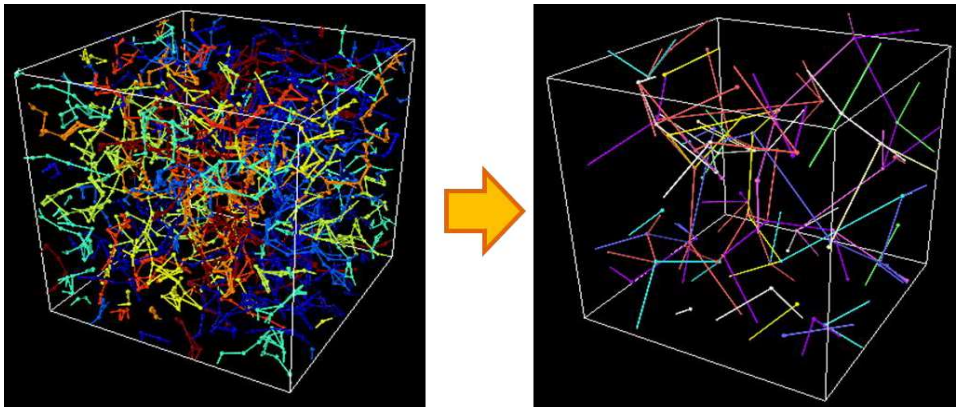

Figure 13 Illustration of the primitive path analysis: The free chain network of the polymer model was simplified as the shortest path connecting fixed chain ends constrained by entanglements with nearby polymer chains.

Table 2 Polymer chemistry-oriented parameters from initial condition of the molecular model ($\mathbf{n_v}$,N), polymer physics-oriented parameters from PPA (L,a,b) and polymer dynamics parameter from the coarse-grained MD (D_c). For the crosslinked model, the difference of D_c was considered. [a]values of the model was taken from [17].

$\mathbf{n_v}(\mathbf{cm^{-3}})$	N	$\mathbf{L_{pp}}$(Å)	**a**(Å)	**b**(Å)	Sulfur weight %	$\mathbf{D_c}(cm^2/s)$
3.96×10^{18}	2000	707.29	35.38	3.54	0	1.20×10^{-7}
					1	9.61×10^{-8}
					2	8.33×10^{-8}
1.98×10^{18}	4000	1521.7	29.00	3.81	0	1.12×10^{-7}
					1	9.14×10^{-8}
					2	9.03×10^{-8}

3.93×10^{18}[a]	1882[a]	1378[a]	64[a]	6.7[a]	0	1.6×10^{-10}[a]

For the model with the longer chain length, longer Kuhn length and smaller tube diameter was observed, since there are more entanglements and constraints for the longer-chain model. Moreover, in the coarse-grained MD, D_c was also calculated as a smaller value due to the increased restriction for the models. However, more considerable Kuhn length, tube diameter, and much small D_c was found in the previous literature [17]. Such discrepancy was occurred from the difference of the coarse-grained potential and the initial condition of modeling.

3. Implementation of the viscoelastic constitutive equation on FEA

3.1. Incremental formulation of the viscoelastic constitutive equation

In this section, the development of the tube theory-based viscoelastic constitutive equation by Doi-Edward [19] is introduced, and the incremental formulation is proposed. Although the implementation of the viscoelastic Cauchy stress in FEA was proposed in the former literature [16, 17] with molecular simulations, the incremental formulation and the derivation of the material tangent stiffness, i.e., Jacobian, which are necessary for implicit FEA, were not reported. The incremental formulation and the materials tangent stiffness derived in this section were applied to the commercial FEA software, ABAQUS user subroutine, and verified by comparing to results from the Cauchy's direct calculation stress.

The viscoelastic Cauchy stress of the polymer-free chain network was calculated by the tensile force applied to each polymer chain, averaged for a tangent vector γ of chain segment s as Eq. (9).

Herein, the probability distribution function $f(\gamma, s, t)$ which physically implies the probability of the tangent vector γ at the segment s at time t, was adopted to take the average, as shown in Eq. (10). In Eq. (**9**), <*> is an averaging operator and tensile force on the primitive chain is $F_t(L) = 3k_BT/Nb^2$.

$$\sigma^v = n_v \langle \int_0^L F_t(L)\gamma \otimes \gamma ds \rangle_{\gamma,L} = n_v \int_{M(\gamma)} \int_0^L F_t(L)\gamma \otimes \gamma f(\gamma, s, t) ds d\gamma \qquad (9)$$

$$f(\gamma, s, t) = \int_0^t \frac{\partial \Psi(s, t-t')}{\partial t'} dt' \int_{M(\gamma_0)} \frac{1}{4\pi} \delta\left(\gamma - \frac{F(t, t') \cdot \gamma_0}{\|F(t, t') \cdot \gamma_0\|}\right) d\gamma_0 \qquad (10)$$

In Eq. (4), $\Psi(s, t)$ is the probability of the chain segment s would be remained in the reference tube at the original configuration at time t, and F(t,t') is the deformation gradient tensor from time t' to t. $\delta(*)$ is the Dirac delta function, and the integral is calculated for the unit sphere domain to consider every direction of the tangent unit vector, γ and γ_0. $\Psi(s, t)$ depends on the relaxation time of the polymer network, and it was modified to take form as

$$\Psi(s, t) = \sum_{j=1,odd}^{\infty} \frac{4}{j\pi} \sin\left(\frac{j\pi s}{L}\right) E_{\alpha,1}\left[-\left(\frac{j^2 t}{\tau_d}\right)^{\alpha}\right] \qquad (11)$$

where $\tau_d = \frac{L^2}{\pi^2 D_c}$ is the disentanglement time, and the standard Mittag–Leffler function $E_{\alpha,1}$ was introduced in [17] to consider the effect of crosslinks or nonuniform distribution of polymer networks' molecular weight. For the free chain network of the uniformly distributed molecular weight, $\alpha = 1$, and the equation is reduced to the Doi–Edward model [34], since $E_{1,1}(x) = e^x$. Collecting those above equations, viscoelastic Cauchy stress is written as below:

$$\sigma^v = \Xi\langle L^2\rangle \sum_{j=1,odd}^{\infty} \int_0^t \Upsilon\left(j, t', t, \tau_d\right) dt', \Xi = n_v \frac{3k_B T}{Nb^2} \tag{12}$$

where

$$\Upsilon(j, t', t, \tau_d) = \mathcal{E}(j, t - t', \tau_d)\Lambda(t, t') \tag{13}$$

$$\mathcal{E}(j, t - t', \tau_d) = \frac{8}{\pi^2 \tau_d}\left[-\frac{\partial}{\partial x} E_{\alpha,1}(-y^{-\alpha})\right]_{y=\frac{j^2(t-t')}{\tau_d}} \tag{14}$$

$$\Lambda(t, t') = \int_{M(\Upsilon)} \gamma \otimes \gamma \, d\gamma \int_{M(\gamma_0)} \frac{1}{4\pi} \delta\left(\gamma - \frac{F(t, t') \cdot \gamma_9}{\left\|F(t, t') \cdot \gamma_9\right\|}\right) d\gamma_0 - \frac{1}{3}\underline{\underline{I}} \tag{15}$$

In the above equations, $\underline{\underline{I}}$ is the second–order identity tensor. Li et al. [17] modified Eq. (12) for the particular case of uniaxial elongation with a small strain. In this case, the deformation gradient F(t,t') is expressed as Eq. (16). Therefore, the normal viscoelastic

Cauchy stress along the loading direction is shown as Eq. (17) and (18), as a function of 1−dimensional small strain $\varepsilon(t)$.

$$F(t',t) = \begin{matrix} 1+\varepsilon(t)-\varepsilon(t') & 0 & 0 \\ 0 & 1-\dfrac{\varepsilon(t)-\varepsilon(t')}{2} & 0 \\ 0 & 0 & 1-\dfrac{\varepsilon(t)-\varepsilon(t')}{2} \end{matrix} \tag{16}$$

$$\sigma_{11}^{v} = 2\Xi L_0^2 \sum_{j=1,odd}^{\infty} \left[\int_0^t \Upsilon_1(j,t',t,\tau_d)dt' + \frac{3}{5}\frac{\tau_d}{j^2}\varepsilon(t) \right] \tag{17}$$

where L_0 is the tube length at the reference configuration, and

$$\Upsilon_1(j,t',t,\tau_d) = \left(\frac{8}{\pi^2\tau_d}\left[-\frac{\partial}{\partial y}E_{\alpha,1}(-y^{\alpha})\right]_{y=\frac{j^2(t-t')}{\tau_d}}\frac{3}{5}(\varepsilon(t)-\varepsilon(t')) \right. \tag{18}$$

In the above equations, they proposed the only formulation of Cauchy stress for 1d finite element analysis (FEA). However, there was no derivation of the equation's numerical formulation for application to the implicit analysis of ABAQUS UMAT. Thus, the development of incremental formulation and tangent stiffness will be described precisely in this paper.

Since our molecular models for the PPA had uniform molecular weight distribution, $\alpha = 1$ was adopted. Then, the viscoelastic Cauchy stress in Eq. (17) can be shown as below

$$\sigma_{11}^{v} = C_1 \sum_{j=1,odd}^{\infty} \left[\frac{3}{5} C_2 \int_0^t e^{-\frac{j^2(t-t')}{\tau_d}} \left(\varepsilon(t) - \varepsilon(t') \right) dt' + \frac{3}{5} \frac{\tau_d}{j^2} \varepsilon(t) \right]$$

$$= \sum_{j=1,odd}^{\infty} \left[\frac{3}{5} C_1 \frac{\tau_d}{j^2} \varepsilon(t) + \frac{3}{5} C_1 C_2 \int_0^t e^{-\frac{j^2(t-t')}{\tau_d}} \varepsilon(t) dt' \right. \quad (19)$$

$$\left. - \frac{3}{5} C_1 C_2 \int_0^t e^{-\frac{j^2(t-t')}{\tau_d}} \varepsilon(t') dt' \right]$$

where, $C_1 = 2\Xi L_0^2, C_2 = \frac{8}{\pi^2 \tau_d}$

Eq. (19) has three terms to calculate; each term was separately formulated in this thesis. Since there is no integration in the first term, it does not have any step before the incremental formulations. For the second term, it can be directly integrated for variable t'.

$$\int_0^t e^{-\frac{j^2(t-t')}{\tau_d}} \varepsilon(t) dt' = \frac{\tau_d}{j^2} \left(1 - e^{-\frac{j^2 t}{\tau_d}} \right) \varepsilon(t) \quad (20)$$

For the last term, it contains two other functions of t' to integrate. Therefore, partial integration was performed.

$$\int_0^t e^{-\frac{j^2(t-t')}{\tau_d}} \varepsilon(t') dt'$$

$$= \frac{\tau_d}{j^2} \left[\left(\exp\left(-\frac{j^2(t-t')}{\tau_d} \right) \varepsilon(t') \right) \Big|_0^t - \int_0^t \exp\left(-\frac{j^2(t-t')}{\tau_d} \right) \frac{\partial \varepsilon(t')}{\partial t'} dt' \right] \quad (21)$$

$$= \frac{\tau_d}{j^2} \left[\left(\varepsilon(t) - \exp\left(-\frac{j^2 t}{\tau_d} \right) \varepsilon(0) \right) - \int_0^t \exp\left(-\frac{j^2(t-t')}{\tau_d} \right) \frac{\partial \varepsilon(t')}{\partial t'} dt' \right]$$

In Eq. (20) and (21), the first terms of Eq. (20) and Eq. (21) can be canceled out each other. And also, for the second term in Eq. (21), it is disappeared since initial strain $\varepsilon(0)$ equals 0. Thus, only the second term in Eq. (20) and integration term in Eq. (21) are left, and the arranged form of Cauchy stress is shown below

$$\sigma_{11}^{v} = \frac{3}{5}C_1\frac{\tau_d}{j^2}\sum_{j=1,odd}^{\infty}\left[\varepsilon(t) - C_2\left\{e^{-\frac{j^2 t}{\tau_d}}\varepsilon(t) + \int_0^t e^{-\frac{j^2(t-t')}{\tau_d}}\frac{\partial\varepsilon(t')}{\partial t'}dt'\right\}\right] \quad (22)$$

In incremental form, the above equation can be shown below Eq. (17) for the n+1 increment of a time step.

$$\sigma_{11}^{v}(t^{n+1}) = \frac{3}{5}C_1\frac{\tau_d}{j^2}\sum_{j=1,odd}^{\infty}\left[\varepsilon(t^{n+1}) - C_2\left\{\begin{matrix} e^{-\frac{j^2 t^{n+1}}{\tau_d}}\varepsilon(t^{n+1}) \\ +\int_0^{t^{n+1}} e^{-\frac{j^2(t^{n+1}-t')}{\tau_d}}\frac{\partial\varepsilon(t')}{\partial t'}dt' \end{matrix}\right\}\right] \quad (23)$$

Similar to the above steps of Eq. (20),(21), three terms were formulated separately. For the first term in Eq. (23),

$$A_j^{n+1} = \frac{3}{5}C_1\frac{\tau_d}{j^2}\varepsilon(t^{n+1}) = \frac{3}{5}C_1\frac{\tau_d}{j^2}(\varepsilon(t^n) + \Delta\varepsilon) = A_j^n + \frac{3}{5}C_1\frac{\tau_d}{j^2}\Delta\varepsilon \quad (24)$$

For the second term,

$$\begin{aligned} B_j^{n+1} &= -\frac{3}{5}C_1C_2\frac{\tau_d}{j^2}e^{-\frac{j^2 t^{n+1}}{\tau_d}}\varepsilon(t^{n+1}) \\ &= -\frac{3}{5}C_1C_2\frac{\tau_d}{j^2}e^{-\frac{j^2(t^n+\Delta t)}{\tau_d}}(\varepsilon(t^n) + \Delta\varepsilon) \\ &= e^{-\frac{j^2\Delta t}{\tau_d}}B_j^n - \frac{3}{5}C_1C_2\frac{\tau_d}{j^2}e^{-\frac{j^2(t^n+\Delta t)}{\tau_d}}\Delta\varepsilon \end{aligned} \quad (25)$$

For the last term,

$$C_j^{n+1} = \frac{3}{5}C_1C_2\int_0^{t^{n+1}} \frac{\tau_d}{j^2} e^{-\frac{j^2(t^{n+1}-t')}{\tau_d}} \frac{\partial\varepsilon(t')}{\partial t'} dt'$$
$$= \frac{3}{5}C_1C_2\left[\int_0^{t^n} \frac{\tau_d}{j^2} e^{-\frac{j^2(t^n-t')}{\tau_d}} e^{-\frac{j^2\Delta t}{\tau_d}} \frac{\partial\varepsilon(t')}{\partial t'} dt' \right. \quad (26)$$
$$\left. + \int_{t^n}^{t^{n+1}} \frac{\tau_d}{j^2} e^{-\frac{j^2(t^{n+1}-t')}{\tau_d}} \frac{\partial\varepsilon(t')}{\partial t'} dt'\right]$$

Using the finite difference approach, $\frac{\partial\varepsilon(t')}{\partial t'}$ can be approximated as follows,

$$\frac{\partial\varepsilon(t')}{\partial t'} = \lim_{\Delta t'\to 0}\left(\frac{\Delta\varepsilon(t')}{\Delta t'}\right) = \lim_{\Delta t\to 0}\left(\frac{\Delta\varepsilon}{\Delta t}\right) \quad (27)$$

Plugging Eq. (27) into Eq. (26) and directly integrated,

$$C_j^{n+1} = e^{-\frac{j^2\Delta t}{\tau_d}} C_j^n + \frac{3}{5}C_1C_2\int_{t^n}^{t^{n+1}} \frac{\tau_d}{\Delta t j^2} e^{-\frac{j^2(t^{n+1}-t')}{\tau_d}} \Delta\varepsilon dt'$$
$$= e^{-\frac{j^2\Delta t}{\tau_d}} C_j^n + \frac{3}{5}C_1C_2\frac{\tau_d^2}{\Delta t j^4}\left(1 - \exp\left(-\frac{j^2\Delta t}{\tau_d}\right)\right)\Delta\varepsilon \quad (28)$$

Combining the above terms, viscoelastic stress σ_{11}^v can be expressed as Eq. (29) in incremental form

$$\sigma_{11}^v(t^{n+1}) = \sum_{j=1,odd}^{\infty}\left(A_j^n + e^{-\frac{j^2\Delta t}{\tau_d}}\left(B_j^n + C_j^n\right)\right.$$
$$\left. + \frac{3}{5}C_1\frac{\tau_d}{j^2}\left[\frac{\tau_d}{j^2} - C_2\left\{e^{-\frac{j^2t^{n+1}}{\tau_d}} + \frac{\tau_d}{\Delta t j^2}\left(1 - \exp\left(-\frac{j^2\Delta t}{\tau_d}\right)\right)\right\}\right]\Delta\varepsilon\right) \quad (29)$$

In the above equation, there are $(2 \times j)$ number of state variables for B_j and C_j to be updated at each iteration. To apply for the ABAQUS

user subroutine UMAT, the material Jacobian, i.e., tangent modulus, the stress–strain curve slope should be defined. The Jacobian is calculated as $\frac{\partial \Delta\sigma}{\partial \Delta\varepsilon}$ where $\Delta\sigma$ is a small increment of Cauchy stress and $\Delta\varepsilon$ is a small increment of strain. Therefore, the Jacobian for this constitutive equation is defined as below

$$\frac{\partial \Delta\sigma}{\partial \Delta\varepsilon} = \frac{3}{5} C_1 \frac{\tau_d}{j^2} - \frac{3}{5} C_1 C_2 \left\{ \frac{\tau_d}{j^2} e^{-\frac{j^2 t^{n+1}}{\tau_d}} + \frac{\tau_d^2}{\Delta t j^4} \left(1 - \exp\left(-\frac{j^2 \Delta t}{\tau_d} \right) \right) \right. \quad (30)$$

3.2. Characterization of the viscoelastic constitutive equation

In this section, Cauchy stress and the materials stiffness derived from the section 3.1 were applied on ABAQUS UMAT. The characteristic parameters listed in

Table 2 were substituted into the viscoelastic constitutive equation. For the simple 1D model composed of 10 bar elements with a total 1m length, a specific sinusoidal form of the strain input was imposed, and stress responses were obtained. Then, dynamic moduli (the storage modulus G' and the loss modulus G") and $\tan\delta$ which

are significant properties to characterize the viscoelastic material, were calculated by investigating the relationship between the input strain and the stress response. The input strain had the functional form of $\varepsilon(t) = \varepsilon_0 \sin(\omega t)$ and the stress response was fitted as $\sigma = \sigma_0 \sin(\omega t + \delta)$. From the relationship between $\varepsilon(t)$ and $\sigma(t)$, the G' and G" were determined as following Eq. (31).

$$G' = \frac{\sigma_0}{\varepsilon_0}\cos\delta, \qquad G'' = \frac{\sigma_0}{\varepsilon_0}\sin\delta, \qquad \tan\delta = \frac{G''}{G'} \tag{31}$$

The storage modulus G' physically means the elastic property of the material (energy storage), it is calculated as the real part, and the loss modulus G" means the viscous part of the material (dissipation of the energy), it is calculated as the imaginary part of the dynamic moduli. The $\tan\delta$ is a characterizing parameter of the phase difference between the input strain and the stress response. The amount of viscoelasticity can be characterized by $\tan\delta$ since it is calculated by a ratio of G" to G'. In order to verify the incremental formulation and the material tangent stiffness derived in section 3.1, dynamic moduli and $\tan\delta$ were compared to those from the direct calculation of the Cauchy stress, as expressed in Figure 14.

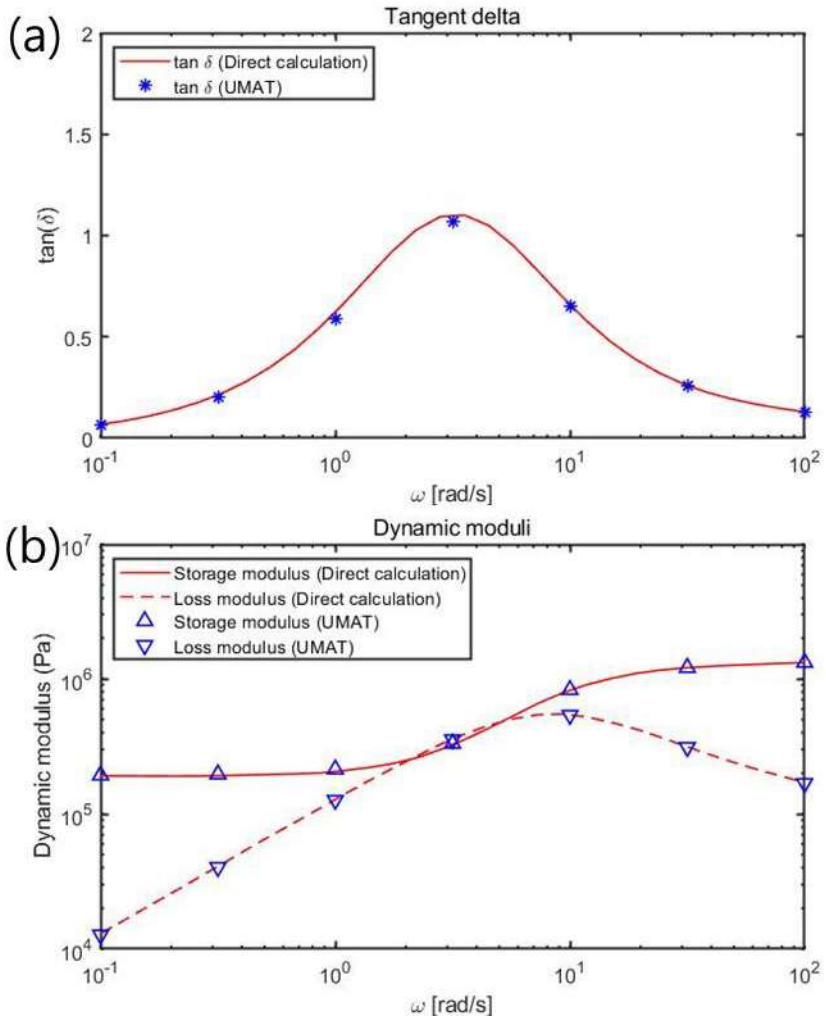

Figure 14 Verification of the incremental formulation and the material tangent stiffness by comparing (a) dynamic moduli and (b) $\tan\delta$ to direct calculation of the Cauchy stress.

3.3. Invetigation of the crosslink effect and a Parametric study of the viscoelastic constitutive equation

In this section, the effect of the crosslink effect on the polymer's viscoelastic properties was studied. The crosslinked elastomer's molecular model was generated by the crosslink algorithm [26] from the initial model that contains randomly dispersed disulfide crosslinkers, the weight percentage of 1,2%. As mentioned in Section 2.4.1, the difference of D_c was applied to consider crosslink effects. When the crosslink density was increased, D_c was reduced due to the restriction of the polymer chain mobility by the crosslinks. As shown in Figure 15, increased dynamic moduli and decreased $\tan\delta$ peak was observed in a higher degree of polymerization and more crosslinked models.

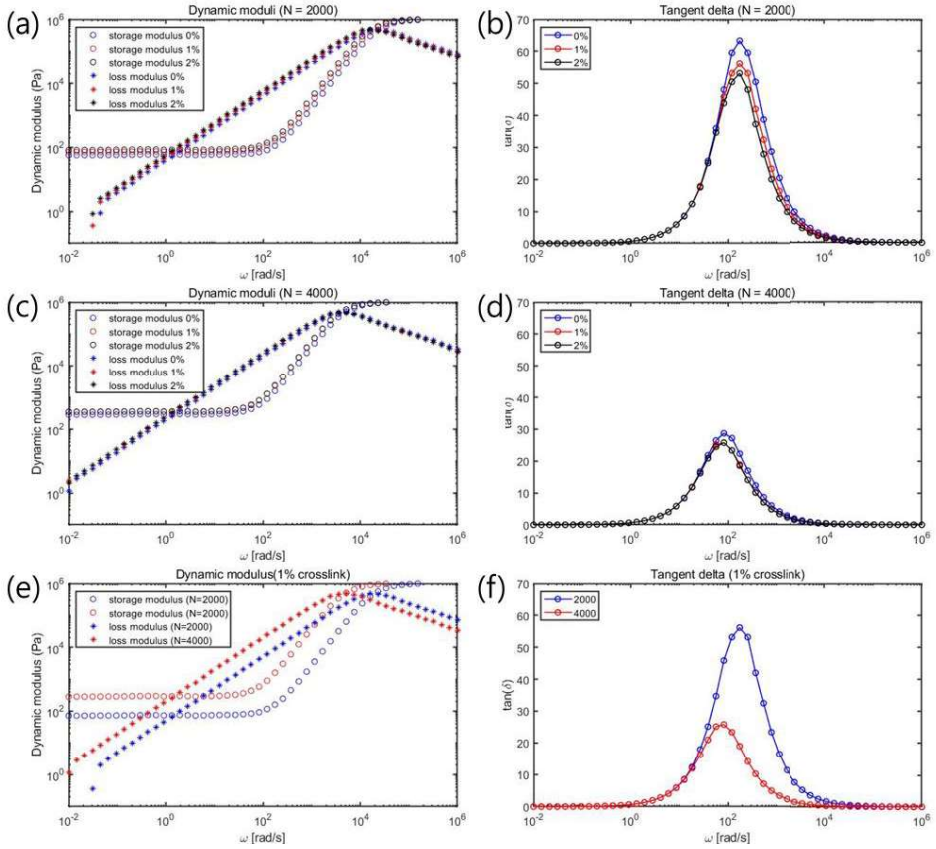

Figure 15 (a) Dynamic moduli, (b) $\tan\delta$ for varying crosslink density (N=2000), (c) Dynamic moduli, (d) $\tan\delta$ for varying crosslink density (N=4000), and (e) Dynamic moduli, (f) $\tan\delta$ for varying chain length (1% crosslinks).

To analyze the above results, the influence of each parameter on the viscoelastic constitutive equation, dynamic moduli and $\tan\delta$ were calculated for varying primitive path length, L and the self diffusivity, D_c was investigated. Since other parameters (a,b,n_v, L)

are only included in Ξ, which is multiplied on the Cauchy stress; they can only affect the magnitude of the dynamic moduli. Thus, the significant parameter which can influence on the intensity of $\tan\delta$ peak is $\tau_d = \frac{L^2}{\pi^2 D_c}$ and the length of primitive path L and self diffusivity D_c were only considered as variables which are included in the τ_d. As reference values, parameters of model 1 in

Table 2 were adopted where it has $L_0 = 707.29\text{Å}$ and $D_{c0} = 1.20 \times 10^{-7}\text{cm}^2/\text{s}$. Dynamic moduli and $\tan\delta$ for $10^1 D_{c0} \sim 10^{-3} D_{c0}$, and $L_0 \sim 20L_0$ are expressed in Figure 16 and Figure 17, respectively.

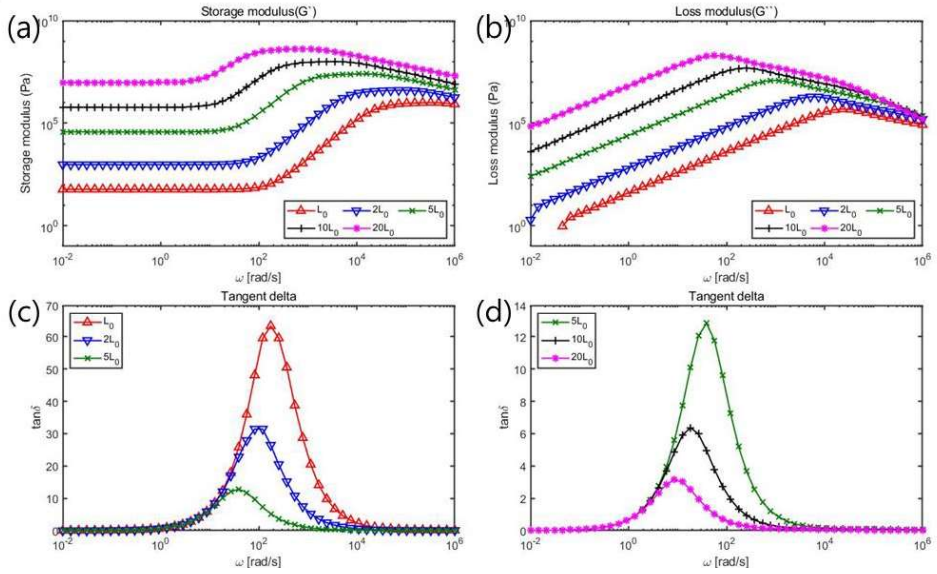

Figure 16 (a) Storage modulus, (b) Loss modulus, (c) $\tan\delta$ for $L_0 \sim 5L_0$ and (d) $\tan\delta$ for $5L_0 \sim 20L_0$ obtained at the frequency of $\omega = 10^{-2} \sim 10^{6} rad/s$ for varying tube length L.

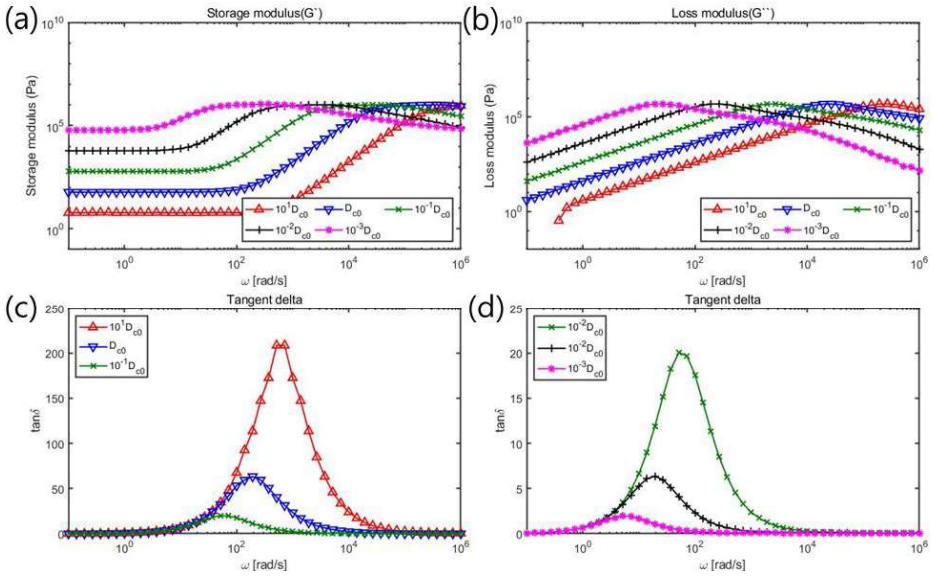

Figure 17 (a) Storage modulus, (b) Loss modulus, (c) $\tan\delta$ for $D_{c0}\sim10^{-2}D_{c0}$ and (d) $\tan\delta$ for $10^{-2}D_{c0}\sim10^{-4}D_{c0}$ calculated at $\omega = 10^{-2}\sim10^{6}rad/s$ for varying self diffusivity D_c.

As shown in the graphs, in the condition of large L and reduced of D_c had led to the rise of dynamic moduli values, and the reduction of $\tan\delta$ peak and frequency at the peak. Since the disentanglement time $\tau_d = \frac{L^2}{\pi^2 D_c}$ is diminished in such conditions, the value of term ε was increased and affected the magnitude of moduli as can be seen in Eq. (8). The reduction of the $\tan\delta$ peak implies a reduction of the dissipated energy, and it was physically compatible that the less mobility of a molecular system and longer polymer chain length led to the reinforcement of elasticity of the polymer system.

4. Conclusions and future works

4.1. Conclusions

In this thesis, the incremental formulation of the 1D viscoelastic Cauchy stress and the material tangent stiffness was derived and verified by comparing dynamic moduli and $\tan\delta$ with those from the direct calculation of the Cauchy stress, which were not reported in the previous literature [17]. In the viscoelastic constitutive equation, the molecular simulations' parameters were substituted that the molecular structure's characteristics can be reflected in the macroscopic FEA. In the viscoelastic constitutive equation, polymer chemistry parameters (n_v,N) determined by the initial condition of the molecular model, polymer physic parameters (a,b,L) calculated from the PPA, and polymer dynamics parameter (D_c) obtained from the coarse-grained MD is included.

To compose a proper coarse-grained potential for PI, the energy renormalization method was adopted. However, the correlation between renormalization parameters (α, β) was not reported in the previous literature [9, 10]. In the higher α condition, higher density and the lower specific volume were observed due to

the reinforcement of the beads' interaction forces. Conversely, in the higher β condition, lower MSD and shear stress were found due to increased average distance between beads. Therefore, to consider the correlation effect and find matching α and β simultaneously, the multi-objective optimization algorithm [21] was adopted in the Arrhenius regime. As a result, the optimized solutions were found as linear sets. The optimized solutions were compatible with the correlation; higher α was needed to compensate for escalated specific volume and MSD in higher β condition. $\alpha(T)$ as a function of the temperature was fitted as the sigmoidal function, Eq. (3). Then, $\beta(T)$ was found as Eq. (8) by matching the density, and $\alpha(T), \beta(T)$ were verified by comparing MSD to the all-atom model. Since the optimization algorithm to consider correlation effect was adopted in addition to the previous energy renormalization method [9], the enhancement of the correctness of the coarse-grained potential is expected.

Comparing PPA and coarse-grained MD results from this thesis to those of the previous literature [17], higher viscoelasticity was shown due to the difference of D_c. To obtain the smaller value

of D_c under $10^{-9}cm^2/s$, calculation through the relation of $D_c \propto N^{-2}$ [19] should be imposed, rather than the direct coarse-grained MD simulations, since it needs huge simulation times and difficult to be achieved in current state of nano-scale MD simulations. To investigate crosslink effect on the viscoelasticity of the polymer, difference in D_c was considered to obtain dynamic moduli. Owing to the restrictions of the polymer chains, D_c was found as lower value in the crosslinked models while other parameters from molecular simulations were used same value as the corresponding free chain models with the same N.

From the coarse-grained MD simulation and the PPA, the characteristic molecular parameters were obtained and plugged into the 1D viscoelastic constitutive equation and the dynamic moduli, $\tan\delta$ were calculated through the relationship between the sinusoidal strain input and the stress response. As a result, the models with a higher degree of polymerization and crosslink density has a lower level of viscoelasticity. Furthermore, the influence of the molecular parameters on the viscoelastic constitutive equation was investigated. Through the parametric study, strengthen of the dynamic moduli and

weakening of the viscoelasticity was found in the longer primitive path length L, and smaller D_c conditions.

4.2. Future works

As a subsequent study for the viscoelastic constitutive equation [17], the combination of the nonaffine hyperelasticity [35], and the Doi-Edward viscoelasticity [19] was conducted in 2016 [36]. However, it was conducted for the 2D FEA for a certain case of the deformation gradients. Therefore, for future works, the full incremental formulation and the derivation of the material tangent stiffness matrix of 3D Cauchy stress for general deformation will be done. By applying into the implicit FEA and the micro-morphic theory [37, 38], a description of the visco-hyperelasticity of the elasticity will be studied. While studying the effect of the crosslinks on the viscoelastic properties of the polymer, the only effect of D_c was considered in this thesis. Therefore, PPA for crosslinked networks [33, 36] will be conducted in subsequent studies. Furthermore, by applying the optimized energy renormalization method on the viscoelastic constitutive equation, the temperature-dependence of the elastomer's viscoelastic properties and the

examination on the time–temperature superposition principle [39, 40] are going to be conducted, since viscoelastic studies on frequency domains were conducted in the previous literatures [17, 36].

Reference

1. Gibson, R.F., *Principles of composite material mechanics*. 2016: CRC press.
2. Mori, T. and K. Tanaka, *Average stress in matrix and average elastic energy of materials with misfitting inclusions.* Acta metallurgica, 1973. **21**(5): p. 571-574.
3. Maerzke, K.A., et al., *TraPPE-UA Force Field for Acrylates and Monte Carlo Simulations for Their Mixtures with Alkanes and Alcohols.* Journal of Physical Chemistry B, 2009. **113**(18): p. 6415-6425.
4. Reith, D., M. Pütz, and F. Müller-Plathe, *Deriving effective mesoscale potentials from atomistic simulations.* Journal of computational chemistry, 2003. **24**(13): p. 1624-1636.
5. Hattemer, G.D. and G. Arya, *Viscoelastic Properties of Polymer-Grafted Nanoparticle Composites from Molecular Dynamics Simulations.* Macromolecules, 2015. **48**(4): p. 1240-1255.
6. Ma, C., et al., *Molecular insight into the Mullins effect: irreversible disentanglement of polymer chains revealed by molecular dynamics simulations.* Phys Chem Chem Phys, 2017. **19**(29): p. 19468-19477.
7. Groot, R.D. and P.B. Warren, *Dissipative particle dynamics: Bridging the gap between atomistic and mesoscopic simulation.* The Journal of chemical physics, 1997. **107**(11): p. 4423-4435.
8. Hoogerbrugge, P.J. and J.M.V.A. Koelman, *Simulating Microscopic Hydrodynamic Phenomena with Dissipative Particle Dynamics.* Europhysics Letters, 1992. **19**(3): p. 155-160.
9. Xia, W., et al., *Energy-Renormalization for Achieving Temperature Transferable Coarse-Graining of Polymer Dynamics.* Macromolecules, 2017. **50**(21): p. 8787-8796.
10. Song, J., et al., *Energy Renormalization Method for the Coarse-Graining of Polymer Viscoelasticity.* Macromolecules, 2018. **51**(10): p. 3818-3827.
11. Arruda, E.M. and M.C. Boyce, *A three-dimensional constitutive model for the large stretch behavior of rubber elastic materials.* 1993.
12. Bergström, J.S. and M.C. Boyce, *Constitutive modeling of the large strain time-dependent behavior of elastomers.* Journal of the Mechanics and Physics of Solids, 1998. **46**(5): p. 931-954.
13. Miehe, C. and S. Göktepe, *A micro-macro approach to rubber-like materials. Part II: The micro-sphere model of finite rubber viscoelasticity.* Journal of the Mechanics and Physics of Solids, 2005. **53**(10): p. 2231-2258.
14. Park, C., J. Jung, and G.J. Yun, *A multiscale micromorphic model with*

strain rate relationship between MD simulations and macroscale experimental tests and dynamic heterogeneity for glassy polymers. Composites Part B: Engineering, 2020: p. 108439.
15. Park, C., J. Jung, and G.J. Yun, *Multiscale micromorphic theory compatible with MD simulations in both time-scale and length-scale.* International Journal of Plasticity, 2020: p. 102680.
16. Tang, S., M. Steven Greene, and W.K. Liu, *Two-scale mechanism-based theory of nonlinear viscoelasticity.* Journal of the Mechanics and Physics of Solids, 2012. **60**(2): p. 199-226.
17. Li, Y., et al., *A predictive multiscale computational framework for viscoelastic properties of linear polymers.* Polymer, 2012. **53**(25): p. 5935-5952.
18. De Gennes, P.-G. and P.-G. Gennes, *Scaling concepts in polymer physics*. 1979: Cornell university press.
19. Doi, M. and S.F. Edwards, *The theory of polymer dynamics*. Vol. 73. 1988: oxford university press.
20. Kröger, M., *Shortest multiple disconnected path for the analysis of entanglements in two- and three-dimensional polymeric systems.* Computer Physics Communications, 2005. **168**(3): p. 209-232.
21. Deb, K., et al., *A fast and elitist multiobjective genetic algorithm: NSGA-II.* IEEE transactions on evolutionary computation, 2002. **6**(2): p. 182-197.
22. Jung, J., C. Park, and G.J. Yun, *Free radical polymerization simulation and molecular entanglement effect on large deformation behavior.* European Polymer Journal, 2019. **114**: p. 223-233.
23. *Dassault Systèmes BIOVIA, Materials studio, 2017 R2, San Diego: Dassault Systèmes, 2017.*
24. Sun, H., *COMPASS: an ab initio force-field optimized for condensed-phase applications overview with details on alkane and benzene compounds.* The Journal of Physical Chemistry B, 1998. **102**(38): p. 7338-7364.
25. Sun, H., et al., *COMPASS II: extended coverage for polymer and drug-like molecule databases.* Journal of molecular modeling, 2016. **22**(2): p. 47.
26. Park, C., J. Jung, and G. Yun, *Interfacial Characterization of Mineralized Carbon Nanotubes.* COMPOSITES RESEARCH, 2018. **31**(5): p. 282-287.
27. Andersen, H.C., *Molecular dynamics simulations at constant pressure and/or temperature.* The Journal of chemical physics, 1980. **72**(4): p. 2384-2393.
28. Berendsen, H.J., et al., *Molecular dynamics with coupling to an external bath.* The Journal of chemical physics, 1984. **81**(8): p. 3684-

3690.
29. Plimpton, S., *Fast parallel algorithms for short-range molecular dynamics*. 1993, Sandia National Labs., Albuquerque, NM (United States).
30. Hoover, W.G., *Canonical dynamics: Equilibrium phase-space distributions.* Physical review A, 1985. **31**(3): p. 1695.
31. Sun, H., et al., *An ab initio CFF93 all-atom force field for polycarbonates.* Journal of the American Chemical Society, 1994. **116**(7): p. 2978-2987.
32. Park, C. and G.J. Yun, *Characterization of interfacial properties of graphene-reinforced polymer nanocomposites by molecular dynamics-shear deformation model.* Journal of Applied Mechanics, 2018. **85**(9).
33. Li, Y., M. Kröger, and W.K. Liu, *Primitive chain network study on uncrosslinked and crosslinked cis-polyisoprene polymers.* Polymer, 2011. **52**(25): p. 5867-5878.
34. Doi, M., S.F. Edwards, and S.F. Edwards, *The theory of polymer dynamics*. Vol. 73. 1988: oxford university press.
35. Davidson, J.D. and N.C. Goulbourne, *A nonaffine network model for elastomers undergoing finite deformations.* Journal of the Mechanics and Physics of Solids, 2013. **61**(8): p. 1784-1797.
36. Ying, L., et al., *Molecular simulation guided constitutive modeling on finite strain viscoelasticity of elastomers.* Journal of the Mechanics and Physics of Solids, 2016. **88**: p. 204-226.
37. Vernerey, F., W.K. Liu, and B. Moran, *Multi-scale micromorphic theory for hierarchical materials.* Journal of the Mechanics and Physics of Solids, 2007. **55**(12): p. 2603-2651.
38. Vernerey, F., et al., *A micromorphic model for the multiple scale failure of heterogeneous materials.* Journal of the Mechanics and Physics of Solids, 2008. **56**(4): p. 1320-1347.
39. Williams, M.L., R.F. Landel, and J.D. Ferry, *The temperature dependence of relaxation mechanisms in amorphous polymers and other glass-forming liquids.* Journal of the American Chemical society, 1955. **77**(14): p. 3701-3707.
40. Abdel-Goad, M., et al., *Rheological properties of 1, 4-polyisoprene over a large molecular weight range.* Macromolecules, 2004. **37**(21): p. 8135-8144.

국문초록

비정질 고분자의 분자 시뮬레이션 기반 점탄성 구성방정식과 증분 정식화 유도

정 지 원
항공우주공학과
서울대학교 대학원

본 학위논문은 탄성체의 분자 특성이 반영된 탄성체의 점탄성 구성방정식의 구성을 목표로 한다. 기존의 점탄성 구성방정식들은 실험을 통해 결정되어 유한요소 해석에 성공적으로 적용되어왔지만, 분자 구조의 특성을 직접적으로 반영하지 않고 있기 때문에 목표로 하는 고분자의 특성을 위한 분자 구조의 특성을 찾아내기에는 어렵다는 단점이 있다. 점탄성 구성방정식에는 고분자 물리, 화학, 동역학적 변수가 포함된다. 각 고분자 특성 변수는 primitive path analysis, 분자 모델의 구성 조건, coarse-grained 분자동역학(MD) 전산모사 해석으로부터 구해지며, 적절한 coarse-grained 분자동역학 포텐셜을 도출하기 위해 energy renormalization 방법을 사용하였다. Energy renormalization 방법은 온도에 따라 분자 간의 상호작용 변수를 조절하여 기존의 all-atom 분자

동역학 전산모사 해석과 같은 수준의 정밀도를 가지면서 해석 속도를 크게 가속시킬 수 있다. 그러나, 기존의 방법에서는 포텐셜에 포함되는 두 변수 간의 상호 관계성에 대해 고려하지 않았기 때문에, 본 연구에서는 다변수 최적화 알고리즘을 이용하여 포텐셜을 검증하였으며, 이를 검증하였다. 또한 coarse-grained MD와 primitive path analysis를 통해 구한 분자 구조 특성 변수를 대입하여 점탄성 구성방정식으로부터 탄성체의 동적 물성을 도출하였다. 기존의 연구에서는 점탄성 구성방정식의 내연적 유한요소 해석을 위한 정식화 과정을 거치지 않았기 때문에, 본 학위논문에서는 구성방정식의 증분에 따른 정식화와 접선 강성 행렬을 유도하였고, 응력의 직접 계산 결과와 비교하여 이를 검증하였다. 또한, 가류 과정이 탄성체의 점탄성에 미치는 효과와, 점탄성 구성방정식에 포함된 변수들이 동적 물성에 미치는 영향을 조사하여 고분자의 분자 특성이 탄성체의 점탄성에 가하는 영향을 연구하였다.

Keywords : 멀티스케일 시뮬레이션, 분자동역학, 점탄성 고분자, 탄성체, 유한요소 해석

Student Number : 2019-20587